CONCLUDING REMARKS

There is rather good experimental evidence for the existence of a "first plateau" in retarding potential curves of Na^+ at $W=12$ and 10 eV and of a "second plateau" at 12 eV. In addition, the two energy distributions of Na^+ indicated by the first and second plateaus can be nicely explained as resulting from reactions (a) and (b). Although the experimental evidence is weaker for the second plateau at 10 eV and the first and second plateaus at 8 and 6 eV, the data are consistent with the existence of such plateaus.

A long tail at large R (i.e., $R>2995$ V) exists at $W=12$ eV. This tail does not appear in similar curves for $W=6, 8$, and 10 eV. If the tail at 12 eV were due to the formation of Na^+ from reaction (c), a similar tail would not be expected at 6 and 8 eV because the threshold for the reaction is 8.78 eV. The absence of the tail at 10 eV, which is only 1.22 eV from threshold, could be due to a small Q_c at this energy. It is therefore conceivable that Na^+ from reaction (c) was observed at $W=12$ eV. If the tail at 12 eV were due to reaction (b) instead, calculations would give the same Q_0 and Q_a and about a 30% larger Q_b.

*Supported by Advanced Research Projects Agency (Project Defender) through the Office of Naval Research.

[1]J. L. Pack and A. V. Phelps, J. Chem. Phys. 44, 1870 (1966).

[2]R. S. Berry, J. C. Mackie, R. L. Taylor, and R. Lynch, J. Chem. Phys. 43, 3067 (1965).

[3]R. H. Neynaber and S. M. Trujillo, Phys. Rev. 167, 63 (1968).

[4]R. H. Neynaber, S. M. Trujillo, and E. W. Rothe, Phys. Rev. 157, 101 (1967).

[5]S. M. Trujillo, R. H. Neynaber, and E. W. Rothe, Rev. Sci. Instr. 37, 1655 (1966).

[6]By using the 147 data points, the relationship between the fractional standard deviation S and the signal I_3 was found to be $S=0.122\, I_3^{-0.75}$. For the analysis to determine the inflections, the standard deviation of the average value of I_3 at R was obtained from $S/\sqrt{n}$ [Y. Beers, Theory of Error (Addison-Wesley Publishing Company, Inc., Reading, Mass., 1962), p. 30], where n is the number of data points at R.

[7]F. Gilmore, J. Quant. Spectry. Radiative Transfer 5, 369 (1965).

[8]P. K. Rol and E. A. Entemann, J. Chem. Phys., 49, 1430 (1968).

PHYSICAL REVIEW VOLUME 180, NUMBER 1 5 APRIL 1969

Population Distributions. II. Charge-Exchange Capture by Protons Incident Upon Ground-State Atoms*

John R. Hiskes

Lawrence Radiation Laboratory, University of California, Livermore, California 94550

(Received 6 January 1969)

The ratios of the excited captures to the total captures have been computed for charge-exchange collision of protons incident upon each of the elements in their ground state. The calculations have been performed for incident proton energies of 5 to 140 keV and employing a simplified form of the Brinkman-Kramers matrix element. Generally speaking the extremes of behavior of the population distributions occur for charge-exchange collisions with the alkalis and with the inert gases; the population distributions for the other target elements fall smoothly within these extremes. The main variations of the population ratios and the primary trends for different target elements agree reasonably well with available experimental data.

I. INTRODUCTION

In an earlier paper,[1] expressions were given for the cross sections for electron capture by protons incident upon hydrogenlike targets. Using these expressions it was possible to deduce some of the features of the population distributions of the excited atoms formed by protons incident upon different elements. In particular, the calculations showed that the excited-state population ratios

could be expected to vary by an order of magnitude or more for different atomic targets.[2] Hydrogenlike functions have also been employed by other workers in the study of excited-state distributions and with similar results.[3,4] However, the use of hydrogenlike functions to simulate the electrons in the target atoms has several limitations. Generally, it is not possible to approximate suitably both the form of the wave function and the energy level of an atomic electron using only a hydrogenlike function, i.e., using only the effective charge as a parameter. This difficulty tends to become more acute for the heavier elements.

In this paper the results are presented of charge-exchange calculations in which the target electrons are represented using Hartree-Fock (HF) functions. The HF functions, taken in conjunction with certain approximations to the Brinkman-Kramers (BK) prior and post interactions, have been used to carry out a computational survey of the excited-state population distributions which extend over all the elements. These excited-state population ratios have been compared with experimentally determined ratios for protons incident upon several different atomic targets. It is found that these calculations reproduce the main features of the experimental population ratios observed for the alkaline, alkaline-earth and inert-gas targets.

II. QUANTITATIVE DISCUSSION

We develop here the expression for the electron-capture cross section for a proton of mass M_b incident upon a target atom with n electrons and nuclear mass M_a. The Schrödinger equation for this system is a function of the laboratory coordinates for the n electrons, $\vec{r}_{ei}$ (where i ranges from 1 to n), the target nuclear coordinate $\vec{r}_a$, and the proton coordinate $\vec{r}_b$. To specify an initial state and a final state for use in the matrix element, it is necessary to introduce two-coordinate transformations:

$$\vec{R} = (M_a\vec{r}_a + M_b\vec{r}_b + m\sum_{i=1}^{n} r_{ei})/(M_a + M_b + nm),$$

with

$$\vec{\rho} = \vec{r}_b - (M_a\vec{r}_a + m\sum_{i=1}^{n}\vec{r}_{ei})/(M_a + nm),$$

$$\vec{r}_i = \vec{r}_{ei} - \vec{r}_a \quad (n \text{ Eqs.}) \tag{1a}$$

and

$$\vec{\sigma} = (M_a\vec{r}_a + m\sum_{i=1}^{n}{}'\vec{r}_{ei})/[M_a + (n-1)m] - (M_b\vec{r}_b + m\vec{r}_{ek})/(M_b + m),$$

$$\vec{r}_i = \vec{r}_{ei} - \vec{r}_a \quad (n-1 \text{ Eqs.}); \quad \vec{s}_k = \vec{r}_{ek} - \vec{r}_b. \tag{1b}$$

The prime on the summation in Eqs. (1b) implies that the $\vec{r}_{ei} = \vec{r}_{ek}$ coordinate is missing from the sum; the $\vec{r}_{ek}$ will be taken to be the coordinate of the active electron captured by the proton. We shall also have need for the quantities:

$$\vec{\alpha} = -\vec{k}_+ + \vec{k}_0[M_a + (n-1)m]/(M_a + nm),$$

$$\vec{\beta} = -\vec{k}_0 + \vec{k}_+ M_b/(M_b + m),$$

$$\vec{\gamma} = -\vec{k}_0 m/(M_a + nm) + \vec{k}_+ m/[M_a + (n-1)m], \tag{2}$$

$$\vec{k}_0 = \vec{v}_0\hbar^{-1}M_b(M_a + nm)/(M_a + M_b + nm),$$

$$\vec{k}_+ = \vec{v}_+\hbar^{-1}\frac{[M_a + [n-1)m](M_b + m)}{M_a + M_b + nm.}$$

The $\vec{v}_0$ and $\vec{v}_+$ are the initial and final relative velocities, respectively.

Upon introducing the center-of-mass transformation, $\vec{R}$, and Eq. (1a) into the complete Schrödinger equation for the system, the center-of-mass motion is separated and the remaining terms which describe the internal motions can be grouped into three categories: a kinetic term describing the relative motion of the incident proton and target atom, a group of terms interpreted as the Schrödinger equation for an n-electron system centered about nucleus M_a, and a collection of interaction terms:

$$V^{\text{prior}} = -\sum_{i=1}^{n}{}'\frac{e^2}{|\vec{r}_b - \vec{r}_{ei}|} + \frac{e^2 n}{|\vec{r}_a - \vec{r}_b|}$$

$$V^{\text{prior}} = -\sum_{i=1}^{n} e^2 \times\left|\vec{\rho} - \vec{r}_i\frac{M_a + (n-1)m}{M_a + nm} + \frac{m}{M_a + nm}\sum_{j=1}^{n}{}'\vec{r}_j\right|^{-1} + e^2 n\left|\vec{\rho} + \frac{m}{M_a + nm}\sum_{i=1}^{n}\vec{r}_i\right|^{-1}. \tag{3}$$

The prime in the j summation implies that the $j = i$ term is absent. The first term in Eq. (3) is the Coulomb interaction between the incident proton and target electrons, and the second term is the proton-nuclear interaction. Initially, for large proton-atom separation, V^{prior} can be neglected and the solution for the remaining terms is taken to be

$$\psi_0(\vec{r}_1, \ldots, \vec{r}_n)\exp(i\vec{k}_0 \cdot \vec{\rho}), \tag{4}$$

where ψ_0 is the Hartree-Fock solution for the target atom.

Alternatively, if one introduces Eqs. (1b) into the Schrödinger equation there results instead a kinetic term describing the relative motion of the outgoing hydrogen atom and the residual atomic ion, a group of terms describing an $(n-1)$-electron system centered about M_a, and a collection of interaction terms:

$$V^{\text{post}} = \frac{-e^2 n}{|\vec{r}_a - \vec{r}_{ek}|} - \sum_{i=1}^{n}{}' \frac{e^2}{|\vec{r}_{ei} - \vec{r}_b|} + \sum_{i=1}^{n}{}' \frac{e^2}{|r_{ei} - \vec{r}_{ek}|} + \frac{e^2 n}{|r_a - \vec{r}_b|},$$

$$V^{\text{post}} = \frac{-e^2 n}{r_k} - \sum_{i=1}^{n} e^2 \left| \vec{\sigma} + \vec{r}_i \frac{M_a + (n-2)m}{M_a + (n-1)m} - \frac{m}{M_a + (n-1)m} \sum_{i=1}^{n}{}'' \vec{r}_j + \frac{\vec{s}_k m}{M_a + m} \right|^{-1} + \sum_{i=1}^{n}{}' \frac{e^2}{|(\vec{r}_i - \vec{s}_k) + (\vec{r}_a - \vec{r}_b)|} + \frac{e^2 n}{|\vec{r}_a - \vec{r}_b|}. \tag{5}$$

The prime indicates the k term is missing from the sum and the double prime means both the i and k terms are missing. The successive terms in Eq. (5) are identified as follows: the interaction between the target nucleus and active electron, the interaction between the proton and residual electrons in the target, the active electron and residual electrons in the target, the active electron and residual target electron interactions, and the interaction between the target nucleus and proton. For large separation of target ion and outgoing hydrogen atom the terms in V^{post} can be neglected and the asymptotic solution is taken to be

$$\psi_+(\vec{r}_1, \ldots, \vec{r}_n)\phi(\vec{s}_k, nlm)\exp(i\vec{k}_+ \cdot \vec{\sigma}), \quad (i \neq k) \tag{6}$$

the product of a target ion function, hydrogenic function, and outgoing plane wave. Solutions (4) and (6) serve as initial and final states, respectively.

Using the definitions given in Eqs. (1) and (2), we have

$$\vec{k}_0 \cdot \vec{\rho} - \vec{k}_+ \cdot \vec{\sigma} = \vec{\alpha} \cdot \vec{r}_k + \vec{\beta} \cdot \vec{s}_k + \sum_{i=1}^{n}{}' \vec{\gamma} \cdot \vec{r}_i, \quad (i \neq k); \tag{7}$$

the Born matrix element can now be written as

$$M_k = \int \psi_+^*(\vec{r}_1, \ldots, \vec{r}_n)\psi_0(\vec{r}_1, \ldots, \vec{r}_k, \ldots \vec{r}_n) \times \phi^*(\vec{s}_k, nlm) V \exp i\left(\vec{\alpha} \cdot \vec{r}_k + \beta \cdot \vec{s}_k + \sum_{i=1}^{n}{}' \vec{\gamma} \cdot \vec{r}_1\right) \times d\vec{r}_1 \cdots d\vec{r}_n d\vec{s}_k, \tag{8}$$

with V assuming the form of either Eq. (3) or (5).

Equation (8) is too complex to make feasible a survey of the population distributions for all the elements. In the spirit of the BK approximation we can simplify V somewhat if we ignore the nucleus-nucleus terms in Eqs. (3) or (5). The first term in Eq. (3) can be divided into two parts: the Coulomb interaction of the incident proton and the active electron, and a sum of terms giving rise to a polarization of the remaining $(n-1)$ target electrons by the incident proton. Neglecting these polarization terms, V^{prior} is approximated by

$$V^{\text{prior}} \approx -e^2/s_k. \tag{9a}$$

A similar approximation for Eq. (5) can be obtained by ignoring the polarization of the residual atomic ion by the outgoing hydrogen atom and approximating the first three terms by

$$V^{\text{post}} \approx -e^2/r_k; \tag{9b}$$

that is, a Coulomb interaction between the active electron captured by the proton and a residual ion of unit charge.

One might suspect that the failure to include the nucleus-nucleus terms and the polarization terms in Eq. (8) would lead to a serious error in the cross section for charge exchange. But, as we shall see in a later section, comparison of experimental data with the calculation based on Eq. (9) suggests that neglecting these terms will not seriously affect the magnitudes of the population ratios.

With the approximation Eq. (9) we proceed by considering first the integration over the coordinates of the $(n-1)$ electrons which remain with the target ion. Adopting the notation of Condon and Shortley,[5] the expressions for ψ_0 and ψ_+^* are taken to be

$$\psi_0 = [n!]^{-1/2} P \mu_1(a^1)\mu_2(a^2)\cdots\mu_n(a^n), \tag{10a}$$

and

$$\psi_+^* = [(n-1)!]^{-1/2} P \mu_1(a^1)\mu_2(a^2)\cdots\mu_n(a^n); \tag{10b}$$

the $\mu_1(a^1)$ are Hartree-Fock orbitals and P is an

antisymmetrizing operator; the ψ_0 and ψ_+* products differ only in that ψ_+* does not contain μ_k*(a^k).

From the definition of $\vec{\gamma}$ in Eq. (2) we would expect its magnitude to be small. Retaining only lowest-order terms in the expansion for γ^2, gives

$$\gamma^2 a_0^2 = \tfrac{1}{2}\left[(m/M_a)^2 + m/M_b)^2\right] \times \left[M_b/(M_a + M_b)\right]^2 m^2 a_0^2 v_+^2/\hbar^2 . \quad (11)$$

For the range of velocities of interest, $m^2 a_0^2 v_+^2/\hbar^2 \approx 1$, and $\gamma^2 a_0^2$ of order m/M_a, we can write

$$\exp\left(i \sum_{i=1}^{n}{}' \vec{\gamma}\cdot\vec{r}_i\right) \simeq 1 + i \sum_{i=1}^{n}{}' \vec{\gamma}\cdot\vec{r}_1 . \quad (12)$$

Upon performing the integrations over the $n-1$ electron coordinates and using the expansion Eq. (12) the matrix element for capture of the kth electron from the orbital with quantum numbers a^k becomes

$$\mathfrak{M}_k = n^{-1/2}\int \phi^*(\vec{s}_k, nlm)\mu_k(a^k)V \times \exp i(\vec{\alpha}\cdot\vec{r}_k + \vec{\beta}\cdot\vec{s}_k)\, d\vec{r}_e d\vec{s}_k - i\gamma n^{-1/2}\int \phi^*(\vec{s}_k, nlm)\left(\sum_{j=1}^{n}{}' D_{jk}\mu_k(a^j)\right) \times V \exp i(\vec{\alpha}\cdot\vec{r}_k + \vec{\beta}\cdot s_k)\, d\vec{r}_k d\vec{s}_k \quad (13)$$

with

$$D_{jk} = \int \mu^*(a^j)\hat{\gamma}\cdot\vec{r}\mu(a^k)\, d\vec{r} \quad (j \neq k). \quad (14)$$

For the elements up to B_e, the dipole matrix elements Eq. (14) between all occupied orbitals vanish and the second integral in Eq. (13) is zero. For the heavier elements, the D_{jk} will be of order a_0 or less, and in view of Eq. (11) the second term in Eq. (13) will be approximately a factor m/M_a smaller than the first term. In view of the approximations already made in the interaction term V, neglecting the second term in Eq. (13) is warranted.

The probability of capturing the kth electron from the orbital with quantum numbers a^k is proportional to $|\mathfrak{M}_k|^2$; but from the form of Eq. (10) the probability of capturing any one of the other $n-1$ electrons in the target from the orbital $\mu(a^k)$ is given by the same expression as Eq. (13). It follows that the probability of capturing any electron from the orbital $\mu(a^k)$ is then proportional to $n|\mathfrak{M}_k|^2 \equiv |\mathfrak{M}|^2$. Further, if there are $N_{\nu\lambda}$ electrons in the target atom with principal quantum number ν and total angular momentum number λ, the orbital $\mu(a^k)$, with $a^k = \nu\lambda$, will occur $N_{\nu\lambda}$ times in the product Eq. (10a), and the probability of capture of any one of the $N_{\nu\lambda}$ electrons is then proportional to $N_{\nu\lambda}|\mathfrak{M}|^2$. The cross section for capture of an electron with initial quantum numbers $\nu\lambda$ to a state nl is then

$$\sigma(\nu\lambda - nl) = \frac{1}{2\pi} N_{\nu\lambda} \frac{M_b^2(M_a + nm)^2}{(M_a + M_b + nm)^2} \times \hbar^{-4}(v_+/v_0)\int_{-1}^{+1} |\mathfrak{M}(\nu\lambda, nl)|^2 d(\cos\theta).$$

With the definitions $y = \beta^2 a_0^2 + b^2$, $b = 1/n$, and $p = mv_0 a_0 h^{-1}$, the cross section can be written

$$\sigma(\nu\lambda - nl) = \frac{N_{\nu\lambda}(1 + m/M_a)}{(4\pi a_0^2 p^2 e^4)}\int_x^{\infty} |\mathfrak{M}(\nu\lambda, nl)|^2 dy . \quad (15)$$

Evaluating y at $\cos\theta = +1$, and neglecting terms of order m/M_a and m/M_b compared with unity, one finds that for all values of the ratio M_b/M_a, the lower limit of the integral in Eq. (15) can be written

$$x = \tfrac{1}{4}p^2 + \tfrac{1}{2}(a^2 + b^2) + (b^2 - a^2)^2/4p^2, \quad (16)$$

where a^2 is the ionization potential expressed in Rydberg units required to remove a $(\nu\lambda)$ electron from the target. If several shells in the target are occupied, the total cross section for charge-exchange capture into a state nl is given by

$$\sigma(nl) = \sum_\nu N_{\nu\lambda}\sigma(\nu\lambda - nl). \quad (17)$$

The total cross section for charge exchange then becomes

$$\sigma_{\text{total}} = \sum_{n=1}^{\infty}\sum_{l=0}^{n-1}\sum_{\nu}\sigma(\nu\lambda - nl). \quad (18)$$

Equation (18) has been used by Nikolaev[6] for the study of charge-exchange capture on ground-state atoms using the approximation Eq. (9b) to the post interaction and employing Slater-type hydrogenic functions to describe the target electrons.

The excited-state population ratio, $R(n)$, calculated in this paper is defined by

$$R(n) = \left[\sum_{l=0}^{n-1}\sum_{\nu}\sigma(\nu\lambda - nl)\right]\left[\sum_{n=1}^{10}\sum_{l=0}^{n-1}\sum_{\nu}\sigma(\nu\lambda - nl)\right]^{-1}. \quad (19)$$

The denominator in Eq. (19) will generally differ from Eq. (18) by a percent or less.

It remains to discuss the evaluation of the in-

tegrals occurring in the matrix element $\mathfrak{M}(\nu\lambda, nl)$. Using the results in Ref. 1, we have, for the prior interaction,

$$|\mathfrak{M}(\nu\lambda,nl)|^2_{\text{prior}} = (2\lambda+1)^{-1} \times \sum_{\mu=-\lambda}^{\lambda} \sum_{l=-m}^{m} \left| \int \mu(\nu\lambda\mu) \exp(i\vec{\alpha}\cdot\vec{r})\, d\vec{r} \right|^2 \times \left| \int \phi(nlm)(e^2/s)\exp(i\vec{\beta}\cdot\vec{s})\, d\vec{s} \right|^2 = (\pi^3/2)e^4 a_0 (2l+1) y^2 F^2(nl;y) \times \left| \int R_{\nu\lambda} P_\lambda \exp(i\alpha r\cos\theta)\, r^2 dr\, d(\cos\theta) \right|^2; \quad (20a)$$

and, for the post interaction,

$$|\mathfrak{M}(\nu\lambda,nl)_{\text{post}}|^2 = (2\lambda+1)^{-1} \times \sum_{\mu=-\lambda}^{\lambda} \sum_{l-m}^{m} \left| \int \mu(\nu\lambda\mu)\left(\frac{e^2}{r}\right)\exp(i\alpha\cdot\vec{r})\, d\vec{r} \right|^2 \times \left| \int \phi^*(nlm)\exp i\vec{\beta}\cdot\vec{s})\, d\vec{s} \right|^2 = 2\pi^3(2l+1)a_0{}^3F^2(nl,y) \times \left| \int R_{\nu\lambda} P_\lambda (e^2/r)\exp(i\alpha r\cos\theta)\, r^2 dr\, d(\cos\theta) \right|^2. \quad (20b)$$

Here the $R_{\nu\lambda}$ are the radial part of the Hartree-Fock function, and P_λ the Legendre function. For the $R_{\nu\lambda}$ we have used either the Tubis,[7] Clementi,[8] or Herman-Skillman (HS)[9] functions. The Clementi functions have the form

$$R_{\nu\lambda} = \sum_j A_j(\nu\lambda) r^{-B_j} \exp(-C_j r), \quad (21a)$$

and are available for all the elements up to krypton. The HS functions are tabulated numerically. For the elements heavier than krypton, HS functions have been fit to functions of the form

$$R_{\nu\lambda} = \prod_{j=1}^{\nu-\lambda-1} (r - r_j) \sum_{i=1}^{4} a_i \exp(-k_i r). \quad (21b)$$

With the expression Eq. (21) for $R_{\nu\lambda}$, the integrals in Eq. (20) can be evaluated by successively differentiating the equation

$$\int \frac{1}{r}\exp\left(i\alpha r\cos\theta - \frac{kr}{a_0}\right) d\vec{r} = \frac{4\pi a_0{}^2}{(\alpha^2 a_0{}^2 + k^2)} \quad (22)$$

with respect to α and k. Notice that with the analytic expression Eq. (21) for $R_{\nu\lambda}$, the cross section Eq. (15) can be expressed as polynomial in x. The primary interest here, however, is for numerical values of the population ratios, and the calculation of the population ratios is greatly facilitated by performing the integral over y in Eq. (15) numerically.

III. DISCUSSION

The cross sections Eq. (15) and the population ratios Eq. (19) have been calculated for incident proton energies ranging from 5 keV up to 140 keV and using either the prior or the post interactions given by Eq. (9). It is in this energy range that the population ratios exhibit their major variations as functions of the principal quantum number, target atom, and proton energy. In this low energy range only a few of the outer shells of electrons in the target atom will contribute significantly to the total cross section. This can be seen by inspecting the expression Eq. (15). For the inner shells, a^2 is large compared with p^2, and contributions to Eq. (15) occur for relatively large values of the variable y. Since the integral over

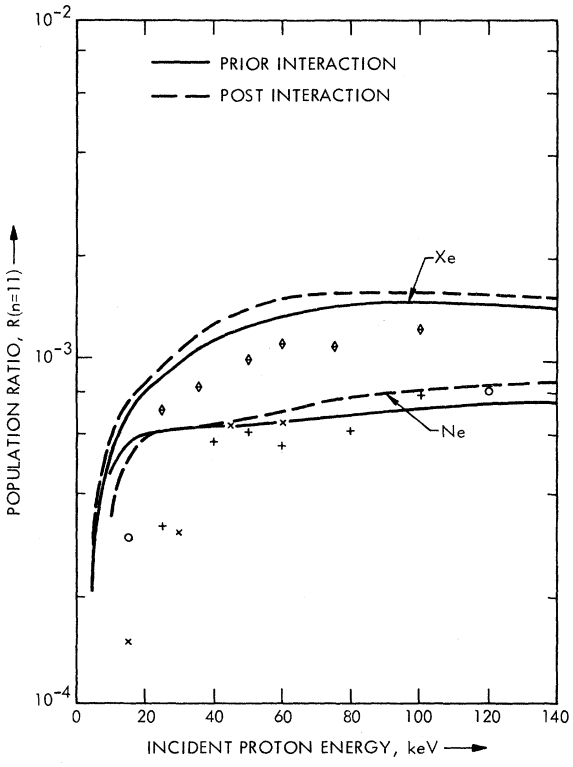

FIG. 1. Comparison of the population ratios, $R(11)$, computed using the prior and post interactions for protons incident upon the $2s^2 2p^6$ configuration of Ne and the $4d^{10}5s^2 5p^6$ configuration of Xe. Also shown for comparison are the experimental values: ◇-Xe data of Ref. 12; +-Ne data of Ref. 12; ○-Ne data of Ref. 10; X-Ne data of Ref. 11 (see text).

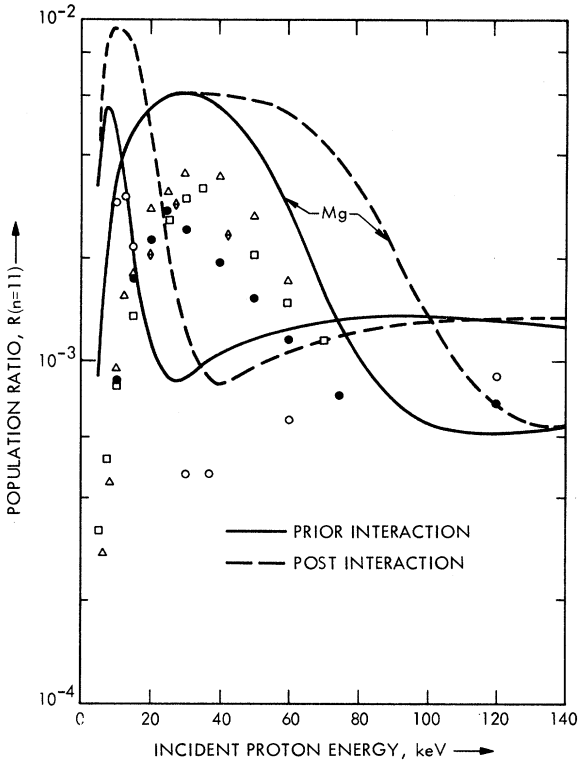

FIG. 2. Comparison of the population ratios, $R(11)$, for protons incident upon the $4d^{10}4s^25p^66s$ configuration of Cs and the $2s^22p^63s^2$ configuration of mg. ○-Cs data of Ref. 10. ● -Mg data of Ref. 10; □ -Mg data of Ref. 11 (see text); △ -Mg data of Ref. 12; ◇ -Mg data of Ref. 14.

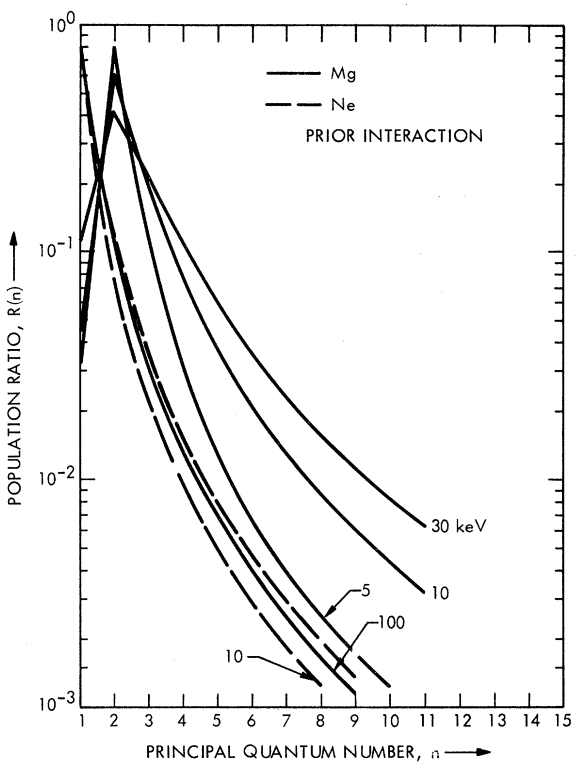

FIG. 3. Population ratio, $R(n)$, versus principal quantum number for protons incident upon the $2s^22p^63s^2$ configuration of Mg for proton energies of 5, 10, 30, and 100 keV. Dashed curves: ratios for 10-and 100-keV protons incident upon $2s^22p^6$ Ne.

$R_{\nu\lambda}$ in Eq. (20) varies approximately as y^{-4} for large y, these contributions are necessarily relatively small. For higher energies, where $x \approx p^2/4$ for all shells, the relative contributions from the inner shells would be expected to be more important.

Examination of the population ratios computed here shows that, broadly speaking, the extremes of behavior occur for protons incident upon the alkalis and for protons incident upon the inert gases, with the population ratios for the other target elements falling smoothly within these extremes. In Fig. 1 we have plotted the population ratio, $R(n=11)$, for protons incident upon two of the inert gases, neon and xenon, and compared these ratios with the experimental values.[10-12] For neon only the $2p^6$ electrons contribute significantly to the ratio, while for xenon, contributions from the $5p^6$, $5s^2$, and $4d^{10}$ electrons are important. In Ref. 11 the neon data is given for $R(n=6)$; the values shown in Fig. 1 have been multiplied by $(\frac{6}{11})^3$. There is seen to be no appreciable difference between the prior and the post ratios. In comparison with the experimental data, the calculated ratios tend to lie above the experimental points at the low end of the energy range.

In Fig. 2 the population ratio is shown for protons incident upon cesium and magnesium where account is taken of the $6s$, $5p^6$, $5s^2$, and $4d^{10}$ target electrons in Cs and the $2s^2$ $2p^6$ $3s^2$ configuration in Mg; the difference between the prior and post results here is more marked than in the case of the inert gases, although the main variations of the population ratios are similar for the two interactions; in all cases the prior ratios lie closer to the experimental data. The data of Ref. 11 for $R(6)$ have been adjusted here according to Fig. 3.

The distinctive feature of the ratios is the pronounced maximum at low energies falling to a distinct minimum at intermediate energies, features which are characteristic of both the theoretical and the experimental[10-14] data. These variations are due mainly to the contribution from the outer $6s$ electron. The origin of the variations shown in Fig. 2 can be better understood by plotting $R(n)$ as a function of n for several different energies as is shown in Fig. 3 for Mg. At very low energies only a few percent of the captures occur into the ground state, and the distribution falls off steeply for large n. This steep distribution accounts for the decline in $R(11)$ for energies below 10 keV

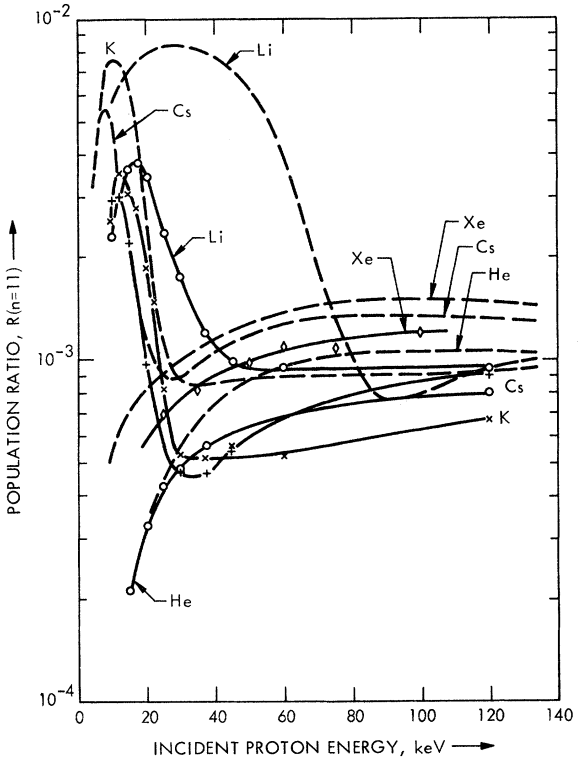

FIG. 4. Comparison of some experimental population ratios with ratios calculated using the prior interaction. ○-Li data, X-K data, +-Cs data, ○-He data, Ref. 10; ◇ -Xe data, Ref. 12; --, calculated ratios.

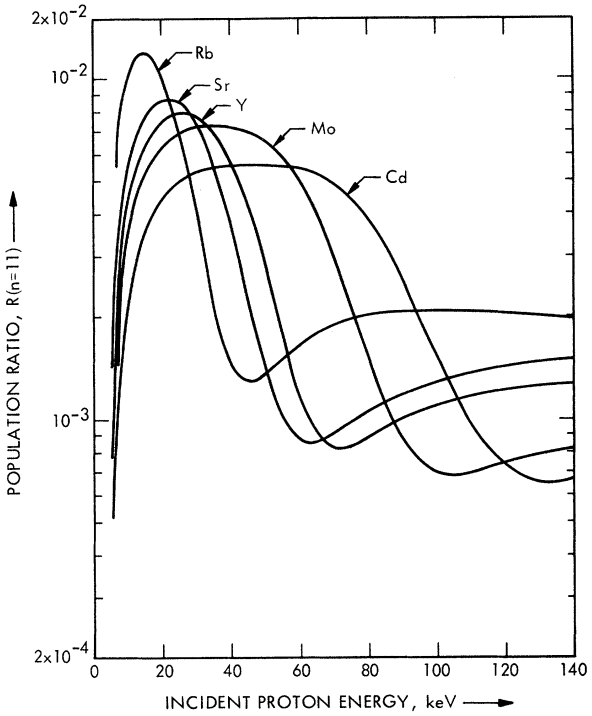

FIG. 5. Comparison of the population ratios for five of the 11 members of the 5s-electron sequence beginning with Rb and ending with Cd. In each case account is taken only of the 5s-electrons in the target.

shown in Fig. 2. At about 20–30 keV and higher the relative captures into the highly excited states has increased, and the distribution for large n varies approximately as n^{-3}. As the incident proton energy is increased from 5 keV up to 100 keV, the relative capture into the ground state increases rapidly, causing the minimum in $R(n = 11)$ near 100 keV shown in Fig. 2. This pattern for Mg is reproduced for all targets in which an outer s electron is captured from the target provided the s electron is not in a 1s orbital. To the extent that these outer s electrons contribute to the total capture, the observed ratio $R(n > 6)$, will exhibit the peaked structure found for Mg and Cs.

Also shown in Fig. 3 is the population ratio $R(n)$ for protons incident upon neon. In the case of a neon target, $R(n)$ is seen to vary monotonically with n in contrast to the s electron captures. This monotonic variation is characteristic of those targets in which the primary contribution to the capture is due to outer p or d electrons.

In Fig. 4 we have compared the population ratios for several target elements for which there is experimental data available[10, 12] with the population ratios computed using the prior interaction. Although differences in magnitude for the calculated and experimental data occur, the trends of the population ratios among the elements for the theoretical data taken together are reproduced by the trends for the experimental data when taken together. Notice that in all cases the computed population ratios tend to fall below the experimental values at the lower energies.

The systematic calculation of the population ratios for protons incident upon all the elements is facilitated by arranging the target elements in sequences according to similar electronic (chemical) properties. In the energy range studied the major contributions to $R(n)$ are due to the outer electrons, and the sequences were selected according to the successive filling of the outer electronic shells (Table 2[14] in Condon and Shortley's book[5] is particularly useful for this purpose). The population ratios were calculated taking into account contributions only from that particular target electron which gave the largest value for $R(n)$. For the alkali sequence these are from the νs electrons, where ν ranges from two through six, and for the alkaline earths from the νs^2 electrons where ν ranges from three through seven. Three other s-electron sequences are the following: the 4s sequence, beginning with potassium and calcium then continuing from scandium through zinc, this later group corresponding to the successive filling of the 3d shell; the 5s sequence beginning with rubidium and

strontium and continuing from yttrium through cadmium (palladium is excluded here because the ground state does not contain a 5*s* orbital but corresponds instead to a filled 4*d* shell); and 6*s* sequence beginning with cesium and barium and continuing from lanthanium through mercury (this group includes the 14 rare-earth elements cerium through lutetium). For the five sequences corresponding to the successive filling of the 2*p*, 3*p*, . . . , 6*p* shells, contributions from the outer *s* and *p* electrons are comparable, at least for the leading members, and these sequences are grouped separately from the above-mentioned *s*-electron sequences.

The population ratios for the alkali and 6*s*-electron sequences are given elsewhere[15, 16]; the $R(n)$ for the 5*s* sequence is shown in Fig. 5. Upon examining the population ratios one will notice that the height of the maximum diminishes and the width of the maximum broadens as the ionization potential of the target increases. This variation is a feature of all the *s*-electron sequences. Also, for each of the *s*-electron sequences the maximum of $R(n)$ is found to vary inversely with ionization potential, excepting for cesium in the alkali sequence; this variation can be used for interpolating the $R(n)$ for the intervening members of the sequences not shown in the figures. A more extensive presentation of the variations of the population ratios for the different elements is given by Hiskes.[17]

The population ratio $R(n)$ is a function of four parameters: the principal quantum number ν and angular momentum λ of the target electron, the incident proton energy, and the principal quantum number n of the captured electron in the outgoing atom. If we were to restrict $R(n)$ to be a function of only two parameters it would be possible to draw $R(n)$ as a continuous contour. The level $n = 11$ is accessible in the electric ionization experiments, and the variations of $R(n = 11)$ are typical of the distribution above about $n = 5, 6$ as is suggested by Fig. 3. Accordingly, we shall eliminate one of the parameters by limiting the discussion to $R(n = 11)$. The $R(n = 11)$ for the *s*-electron sequences have their maxima in the interval from 5 to 30 keV. For those sequences in which the *p* electrons or *d* electrons in the target atom

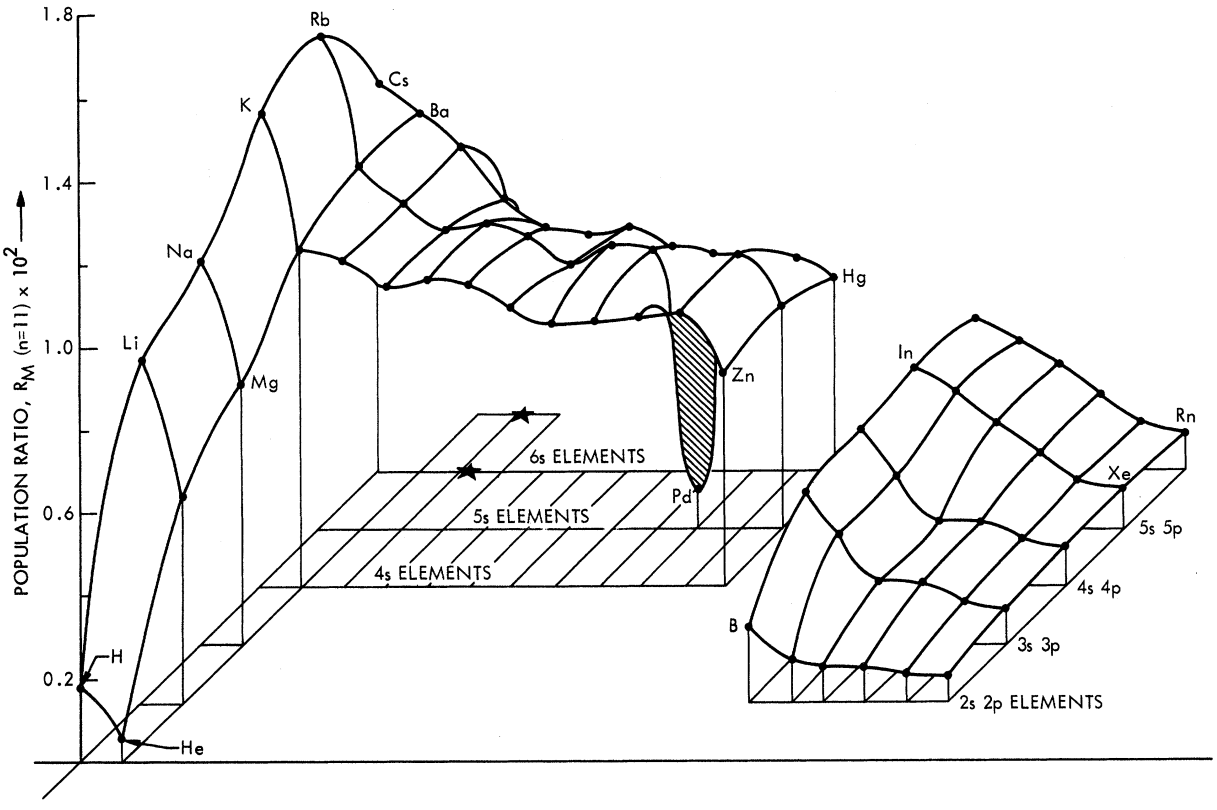

FIG. 6. Contours of the maximum population ratio that occur in the incident proton energy interval $5 < E < 30$ keV plotted aginst the atomic number of the target atom. The contour on the left includes only contributions from the outermost *s* electrons of the target atom to the population ratio; the contour on the right includes contributions from the outermost *s* and *p* electrons. In the case of Pd there are no 5*s* electrons in the ground state; the value of $R_M(11)$ for Pd is derived for captures from the 4*d* shell.

are the main contributors to $R(11)$, the maximum occurs at higher energies as is seen for example in Fig. 1. But for these p and d target atoms the energy dependence of the population ratio is a much less sensitive function of proton energy, and there is no loss of essential features in illustrating the variations among the elements if we compare the $R(11)$ for these p, d targets at 30 keV with the $R(11)$ of the s-electron sequences. To a large degree then, the essential functional dependence of the highly excited population distributions upon the target atom can be displayed by plotting the maximum value of $R(11)$ which occurs in the energy interval 5 to 30 keV as a function of the parameters ν and λ belonging to the outer shell of the target.

Figure 6 shows such a contour in which is plotted the population ratio maximum, $R_M(11)$, as function of ν, λ covering all the elements up to atomic number 104 and using the prior interaction given by Eq. (9a). This contour is a plot of $R_M(11)$ taking into account only the contributions from the outer s electron, and the outermost s and p electrons in the case of the p-electron sequences which are grouped in the contour shown in the right-hand portion of the figure. The principal quantum number ν is plotted along the left-hand abscissae, and the leading abscissa denote the successive filling in of the s and d shells of the s-electron sequences; the leading abscissa for the portion of the figure on the right corresponds to the successive filling of the p shells. The position of the star along the $6s$ sequence locates the rare earths (characterized by the successive filling of the $4f$ shell) which are suppressed on the diagram. The $R_M(11)$ for the rare earths vary about ±15% above and below the contour at this point based upon the variation of the ionization potentials for these elements. The star along the $7s$ element sequence locates the second-row rare-earth elements beginning with thorium and uranium and continuing through the transuranic elements. While the calculations using the post interaction Eq. (9b) have not been as comprehensive as the prior calculations used in constructing the contour of Fig. 6, the main trends and features displayed by the contour are characteristic of either interaction. Inspection of the figure shows that the contour has a ridge running from rubidium through barium then continuing along the $5s$ electron sequence and along the $5s5p$ electron sequence. This ridge beyond barium is a consequence of the increasing ionization potentials of the outer s and p electrons for the elements heavier than lanthanum.

The contour shown in Fig. 6 represents an upper limit to the magnitude of $R_M(11)$. The inclusion of the contributions of the inner shell electrons to the expression (19) would be expected to lower the magnitudes of $R_M(11)$, for as we have seen in Fig. 5 the relative contributions to the highly excited-state cross section are reduced in the case of capture of target electrons with higher ionization potentials. In Fig. 7 is shown the contour for $R_M(11)$ but modified to include effects of the inner shell electrons. The population ratio of the $4s$ electron sequence is reduced substantially by inclusion of contributions from the $3p$ and $3d$ target electrons. The $5s$ sequence is affected by contributions from the $4p$ and $4d$ electrons and the $6s$ sequence by contributions from the $5p$ and $5d$ target electrons. The ionization potentials for the

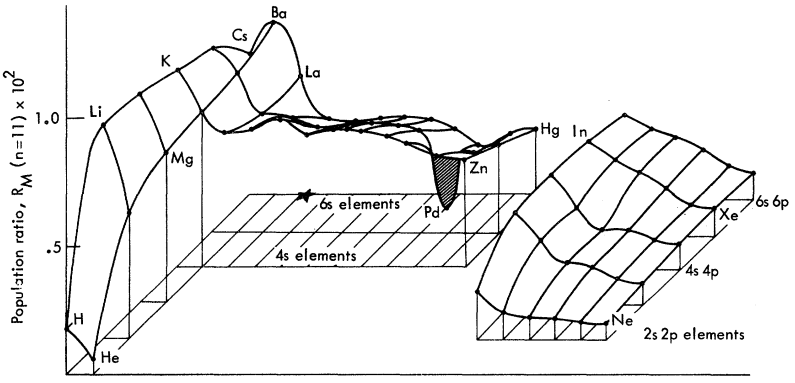

FIG. 7. Contours of the maximum population ratio that occur in the incident proton energy interval $5 < E < 30$ keV plotted against the atomic number of the target atom. These contours include contributions from the inner shell electrons. The position of the rare-earth sequence is indicated by the star along the $6s$ element sequence. For those rare earths with no $5d$ electrons in their ground-state configuration the values of R_M lie between the values shown for La and Ba; for those rare earths with $5d$ electrons the values of R_M will lie between the values for Hf and La.

inner electrons are taken from Charlotte Moore's tables[18] and from Lotz's paper.[19] The ionization potentials for the 4*d* and 5*d* electrons in the transition element region are taken from the HS tables.[9]

Comparing the contours of Figs. 6 and 7, the effect of the inner shell electrons is to reduce the values for $R_M(11)$ of the heavier alkalis relative to the values for the heavier alkaline earths. Moving along the contour of Fig. 7 from the region of the lighter to the heavier alkalis and alkaline earths, the contour becomes twisted. The largest population ratios persist in the region of the light and intermediate alkalis, in the region of the alkaline earths, and for the leading members of the *p*-electron sequences. Referring back to Figs. 1, 2, and 4, the experimental values for $R_M(11)$ are approximately 20 to 60% less than the theoretical values at the lower end of the energy range; this suggests that by dividing the ordinate of Fig. 7 by a factor of 1.5 one can obtain a semiempirical contour which will reproduce all experimental values to within about 30%.

IV. CONCLUSIONS

The population ratios for electron capture into the highly excited levels ($n > 7$) are a maximum for those target atoms in the region of the light and intermediate alkalis, for the alkaline earths, and for the leading members of the *p*-electron sequences. For those target atoms in which an outer *s*-electron contributes significantly to the capture, this population ratio exhibits a pronounced maximum at low (10–30 keV) incident proton energies, falling to a distinct minimum at intermediate energies. For the intermediate excited states ($2 \leq n \leq 5$) the population ratio has considerable structure at these lower energies, and the capture into the intermediate levels comprises the main portion of the total capture. For those target elements in which the primary contribution to the total capture is due to the *p* or *d* electrons, e.g., the inert gases and palladium the highly excited-state population ratios do not exhibit the low-energy maximum, and the distribution over the intermediate levels falls off monotonically for the entire energy range.

The approximation to the BK matrix element employed here leads to reasonably good estimates for the population ratios for the highly excited states over most of the energy range, but it consistently underestimates the population ratios at the lower end of the energy range.

ACKNOWLEDGMENTS

The author is indebted to Dr. K. H. Berkner, Dr. W. S. Cooper, III, Dr. S. N. Kaplan, and Dr. R. V. Pyle for making available their magnesium and neon data prior to publication.

---

*This work was performed under the auspices of the U.S. Atomic Energy Commission.

[1]J. R. Hiskes, Phys. Rev. 137, A361 (1965).

[2]J. R. Hiskes, Phys. Letters 17, 263 (1965).

[3]S. T. Butler and R. M. May, Phys. Rev. 137, A10 (1965).

[4]R. M. May and J. G. Lodge, Phys. Rev. 137, A699 (1965).

[5]E. V. Condon and E. Shortley, The Theory of Atomic Spectra (Cambridge University Press, Cambridge, New York, 1959).

[6]V. S. Nikolaev, Zh. Eksperim. i Teor. Fiz. 51, 1263 (1966) [English transl.: Soviet Phys. – JETP 24, 847 (1967)].

[7]A. Tubis, Phys. Rev. 102, 1049 (1956).

[8]E. Clementi, IBM J. Res. Develop. Suppl. 9, 2 (1965).

[9]F. Herman and S. Skillman, Atomic Structure Calculations (Prentice-Hall, Inc., Englewood Cliffs, New Jersey, 1963).

[10]R. N. Il'in, V. A. Oparin, E. S. Solovev, and N. V. Fedorenko, Zh. Tekhn. Fiz. 36, 1241 (1966) [English transl.: Soviet Phys. – Tech. Phys. 11, 921 (1967)].

[11]K. H. Berkner, W. S. Cooper, III, S. N. Kaplan, and R. V. Pyle, Lawrence Radiation Laboratory Report, UCRL-18342, 1968 (unpublished).

[12]A. C. Riviere, U.S. Atomic Energy Establishment Report No. AERE-R4818, 1964 (unpublished), p. 124.

[13]A. H. Futch and K. G. Moses, Abstracts of the Fifth International Conference on the Physics of Electronic and Atomic Collisions (Nauka, Leningrad, 1967), p. 12.

[14]A. C. Riviere, Abstracts of the Fifth International Conference on the Physics of Electronic and Atomic Collisions (Nauka, Leningrad, 1967) p. 15.

[15]J. R. Hiskes, Abstracts of the Fifth International Conference on the Physics of Electronic and Atomic Collisions (Nauka, Leningrad, 1967), p. 2.

[16]J. R. Hiskes, Lawrence Radiation Laboratory Report No. UCRL-70219, 1967 (unpublished).

[17]J. R. Hiskes, Lawrence Radiation Laboratory Report No. UCRL-71422, 1967 (unpublished).

[18]C. E. Moore, Atomic Energy Levels, National Bureau of Standards Circular No. 467 (U.S. Government Printing Office, Washington, D.C., 1949–1958), Vols. I, II, and III.

[19]W. Lotz, J. Opt. Soc. Am. 58, 915 (1968).